Progress In Electromagnetics Research, Vol. 122, 311–325, 2012

ANALYSIS OF TOPOLOGICAL DERIVATIVE FUNCTION FOR A FAST ELECTROMAGNETIC IMAGING OF PERFECTLY CONDUCING CRACKS

Y.-K. Ma[1], P.-S. Kim[2], and W.-K. Park[2,*]

[1]Department of Statistics, Seoul National University, Seoul 151-747, Korea

[2]Department of Mathematics, Kookmin University, Seoul 136-702, Korea

Abstract—We consider a topological derivative based imaging technique for non-iterative imaging of small and extended perfectly conducting cracks with Dirichlet boundary condition. For this purpose, we introduce topological derivative imaging function based on the asymptotic formula in the existence of narrow crack. We then mathematically analyze its structure in order to investigate why it yields the shape of crack(s). Analyzed structure gives us an optimal condition to get a better image of them. Various numerical experiments support our analysis.

1. INTRODUCTION

Achieving a reliable imaging of inhomogeneities completely hidden in a material is a difficult problem due to the unavoidable ill-posedness and inherent nonlinearity of the inverse problems. Nevertheless, it is still an interesting one that arises in a number of fields such as physics, medical science, and material engineering, highly related to the human life. Corresponding researches can be found in [2, 4, 7, 9, 11, 12, 14–17, 20–22, 27, 28] and references therein.

Recently, an inverse scattering problem for time-harmonic acoustic, electromagnetic waves from a perfectly conducting crack in two-dimensions $\mathbb{R}^2$ with Dirichlet boundary condition has been considered rigorously in [19]. In this literature, Newton-type iteration method has been suggested for imaging shape of crack. In order to guarantee a successful imaging, one must evaluate complex calculation

Received 29 September 2011, Accepted 16 November 2011, Scheduled 22 November 2011

* Corresponding author: Won-Kwang Park (parkwk@kookmin.ac.kr).

of the Fréchet derivative, apply optimized regularization terms highly depend on the problem and perform with a good initial guess close enough to the unknown crack. Without it, one might suffer from large computational costs with the risk of non convergence issue. Nevertheless, most of algorithm is restricted for imaging of single crack and hard to extend it for the multiple cracks. Therefore, the investigation of both imaging algorithm and mathematical theory for generating a reliable initial guesses must be performed beforehand.

For this purpose, alternative non-iterative imaging algorithms have been developed in order to overcome difficulties of iteration one. Among them, topological derivative based imaging algorithm has been successfully adapted in the imaging of anomalies (such as cracks) and in shape optimization problem, refer to [5–8, 10, 18, 23, 26]. However, in many researches, it has been used heuristically without analysis. Recently, mathematical analysis of topological derivative based imaging algorithm is considered. But it is restricted to the imaging of small electromagnetic inclusions so that an extension of analysis is highly required.

The main purpose of this paper is to analyze topological derivative based imaging function and to explain why it yields the shape of small and extended perfectly conducting cracks. For this purpose, we will apply rigorously derived asymptotic expansion formula due to the existence of small crack.

This paper constructed as follows. In Section 2, the two-dimensional direct scattering problem and topological derivative based imaging function are introduced. A mathematical analysis of topological derivative imaging function is carefully treated in Section 3. In Section 4, numerical simulations for imaging small cracks are illustrated in order to show the effectiveness and applied to the extended arbitrary shaped one. We end this paper with a short conclusion in Section 5.

2. DIRECT SCATTERING PROBLEM AND TOPOLOGICAL DERIVATIVE

Assume that a perfectly conducting crack is completely embedded in a homogeneous domain $\Omega \subset \mathbb{R}^2$. In order to represent this crack, we denote Γ as an oriented piecewise smooth nonintersecting arc without cusp that can be represented as

$$\Gamma = \{\psi(s) : s \in [-1, 1]\} \tag{1}$$

where $\psi : [-1, 1] \longrightarrow \mathbb{R}^2$ is a smooth injective function. Assume that the crack does not touch the boundary $\partial\Omega$ so that it must be located

at some distance from $\partial\Omega$, i.e., there is a nonzero positive constant s such that

$$\text{dist}(\Gamma, \partial\Omega) = s > 0,$$

where dist(A, B) denotes the distance between A and B.

Throughout this paper, we consider the so-called Transverse Magnetic polarization case. Let $\{\theta_1, \theta_2, \ldots, \theta_M\}$ be M equi-distributed directions on the unit circle S^1, $g^{(m)}(x)$, $m = 1, 2, \ldots, M$, be given boundary condition on $\partial\Omega$, and $u^{(m)}(x)$ be the (single-component) electric field that satisfies following boundary value problem

$$\begin{cases} \Delta u^{(m)}(x) + \omega^2 u^{(m)}(x) = 0 & \text{in} \quad \Omega\backslash\overline{\Gamma} \\ u^{(m)}(x) = 0 & \text{on} \quad \Gamma \\ \dfrac{\partial u^{(m)}}{\partial \nu}(x) = g^{(m)}(x) & \text{on} \quad \partial\Omega \end{cases} \tag{2}$$

for a fixed frequency ω. Here, $\nu(x)$ is the unit normal to $\partial\Omega$ at x. Throughout this paper, we suppose ω^2 is not an eigenvalue of (2). Similarly, let $U^{(m)}(x)$ be the solution of Equation (2) without Γ. Then the problem we consider here is the computation of the topological derivative of the energy function depending on the solution $u^{(m)}(x)$:

$$\mathbb{J}(\Omega) := \frac{1}{2}\sum_{m=1}^{M}\int_{\partial\Omega}\left|u^{(m)}(x) - U^{(m)}(x)\right|^2 dS(x), \tag{3}$$

where $|f(x)|^2 = f(x)\bar{f}(x)$ and $\bar{f}(x)$ is complex conjugate of $f(x)$.

In order to compute the topological derivative, let us create a linear crack Σ of small length $2h$ at the point $z \in \Omega$; we denote $\Omega|\Sigma$ as that domain. Then due to the change of the topology of Ω, we can consider the topological derivative $d_T\mathbb{J}(z)$ based on the $\mathbb{J}(\Omega)$ with respect to the point z as follows:

$$d_T\mathbb{J}(z) = \lim_{h\to 0+}\frac{\mathbb{J}(\Omega|\Sigma) - \mathbb{J}(\Omega)}{\phi(h)}, \tag{4}$$

where $\phi(h) \longrightarrow 0$ as $h \longrightarrow 0+$. From the relationship (4), we have the asymptotic expansion:

$$\mathbb{J}(\Omega|\Sigma) = \mathbb{J}(\Omega) + \phi(h)d_T\mathbb{J}(z) + o(\phi(h)).$$

Then topological derivatives $d_T\mathbb{J}(z)$ with M different incident waves at given frequency ω are follows. Derivation of following theorem is similar to the method introduced in [23]. For reader's sake, the proof is written in the appendix.

Theorem 2.1 Topological derivative *The topological derivatives corresponding to the (3) is given by*

$$d_T\mathbb{J}(z) = \mathfrak{Re}\left(\sum_{m=1}^{M} V^{(m)}(z)\overline{U^{(m)}(z)}\right), \tag{5}$$

where $\mathfrak{Re}\,(F)$ *denotes the real part of* F *and* $V^{(m)}\,(x)$ *satisfies adjoint problem:*

$$\begin{cases} \Delta V^{(m)}(x) + \omega^2 V^{(m)}(x) = 0 & \text{in} \quad \Omega \\ \dfrac{\partial V^{(m)}}{\partial \nu}(x) = U^{(m)}(x) - u^{(m)}(x) & \text{on} \quad \partial\Omega. \end{cases} \tag{6}$$

3. ANALYSIS OF TOPOLOGICAL DERIVATIVE BASED IMAGING FUNCTION

At this moment, we analyze the topological derivative based imaging function in (5) when the crack Γ is a line segment of small length $2h$ whose center is located at y. Since $V^{(m)}\,(x)$ satisfies adjoint problem (6), it can be represented as

$$\begin{aligned} V^{(m)}(z) &= \int_{\partial\Omega} \frac{\partial V^{(m)}}{\partial \nu}(x)\mathcal{N}(z,x)dS(x) \\ &= \int_{\partial\Omega} \left(U^{(m)}(x) - u^{(m)}(x)\right)\mathcal{N}(z,x)dS(x) \end{aligned}$$

for $x \in \partial\Omega$ and $z \in \Omega$. Here $\mathcal{N}\,(x,\, z)$ is Neumann function for Ω, the solution to

$$\begin{cases} \triangle\mathcal{N}(x,z) + \omega^2\mathcal{N}(x,z) = -\delta(x,z) & \text{in} \quad \Omega \\ \dfrac{\partial \mathcal{N}(x,z)}{\partial \nu(x)} = 0 & \text{on} \quad \partial\Omega. \end{cases}$$

Due to the existence of small crack, $u^{(m)}\,(x)$ satisfies following asymptotic expansion formula (see [5]): for $x \in \partial\Omega$ and $y \in \Gamma$,

$$u^{(m)}(x) - U^{(m)}(x) = \frac{2\pi}{\ln(h/2)}U^{(m)}(y)\mathcal{N}(y,x) + O\left(\frac{1}{|\ln h|^2}\right).$$

Since h is small enough, the residue term $O(|\ln h|^{-2})$ can be negligible. So by removing residue term and applying this formula to (5) gives

$$d_T\mathbb{J}(z) = -\frac{2\pi}{\ln(h/2)}\mathfrak{Re}\left\{U^{(m)}(y)\left(\int_{\partial\Omega}\mathcal{N}(y,x)\mathcal{N}(z,x)dS(x)\right)\overline{U^{(m)}(z)}\right\}. \tag{7}$$

Now, let us decompose $\mathcal{N}(x, z)$ into singular and regular terms as follows:

$$\mathcal{N}(x,z) = \Phi(x,z) + \mathcal{R}_\Phi(x,z).$$

Here $\Phi(x,z)$ is a two-dimensional two-dimensional time harmonic Green function (or fundamental solution)

$$\Phi(x,z) = -\frac{j}{4}H_0^1(\omega|x-z|),$$

where H_0^1 denotes the Hankel function of the first kind of order 0 and $\mathcal{R}_\Phi(x,z)$ satisfies

$$\begin{cases} \triangle\mathcal{R}_\Phi(x,z) + \omega^2\mathcal{R}_\Phi(x,z) = 0 & \text{in} \quad \Omega \\ \dfrac{\partial\mathcal{R}_\Phi(x,z)}{\partial\nu(x)} = -\dfrac{\partial\Phi(x,z)}{\partial\nu(x)} & \text{on} \quad \partial\Omega. \end{cases}$$

With this, let us consider the following term:

$$\begin{aligned} &\int_{\partial\Omega}\mathcal{N}(y,x)\mathcal{N}(z,x)dS(x) \\ &= \underbrace{\int_{\partial\Omega}\Phi(y,x)\Phi(z,x)dS(x)}_{:=\mathcal{I}_1} + \underbrace{\int_{\partial\Omega}\Phi(y,x)\mathcal{R}_\Phi(x,z)dS(x)}_{:=\mathcal{I}_2} \\ &\quad + \underbrace{\int_{\partial\Omega}\mathcal{R}_\Phi(y,x)\Phi(z,x)dS(x)}_{:=\mathcal{I}_3} + \underbrace{\int_{\partial\Omega}\mathcal{R}_\Phi(y,x)\mathcal{R}_\Phi(x,z)dS(x)}_{:=\mathcal{I}_4}. \end{aligned}$$

Since, $\mathcal{R}_\Phi$ is regular, there is no blow up of $\mathcal{I}_4$. Moreover, since $x \in \partial\Omega$ and $y \in \Gamma$, $\Phi(y,x)$ have no singularity so that there is no blow up of $\mathcal{I}_2$ also. Since $x \in \partial\Omega$ and $z \in \Omega$, $\mathcal{N}(x,z)$ has a singularity at $x = z$. So, in order to evaluate $\mathcal{I}_3$, we must insulate this singularity. For this purpose, we recall that in two-dimensional space, for $\omega|x-z| \to 0$

$$\begin{aligned} \Phi(x,z) \;=\; &\frac{1}{2\pi}\ln|x-z| - \Bigg(\underbrace{\frac{j}{4} - \frac{1}{2\pi}\ln\frac{\omega}{2} - \frac{C}{2\pi}}_{:=C_\omega}\Bigg) \\ &+O(\omega^2|x-z|^2\ln(\omega|x-z|)), \end{aligned}$$

where, C denotes the Euler constant $C = 0.57721566\ldots$ (see [13]). Now, let us fix $r > 0$ and denote $B(x,r)$ as a ball of center x and radius r. Then since $\partial\Omega$ can be partitioned into $\partial\Omega_1 := \partial\Omega\backslash(\Omega \cap \partial B(x,r))$

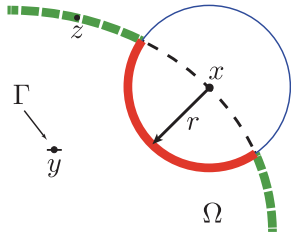

Figure 1. $\partial\Omega_1$ (green dashed line) and $\partial\Omega_2$ (red solid line).

and $\partial\Omega_2 := \Omega \cap \partial B(x, r)$ (see Figure 1), by applying Hölder's inequality

$$\begin{aligned}
|\mathcal{I}_3| &\le \int_{\partial\Omega} |\mathcal{R}_\Phi(y,x)\Phi(z,x)| dS(x) \\
&\le \frac{1}{2\pi} \int_{\partial\Omega} |\mathcal{R}_\Phi(y,x)| \ln|x-z| dS(x) + C_\omega \int_{\partial\Omega} |\mathcal{R}_\Phi(y,x)| dS(x) \\
&\le \frac{1}{2\pi} \max|\mathcal{R}_\Phi(y,x)| \int_{\partial\Omega} \ln|x-z| dS(x) + C_1 \\
&= C_2 \lim_{r\to 0+} \left(\int_{\partial\Omega_1} \ln|x-z| dS(x) + \int_{\partial\Omega_2} \ln|x-z| dS(x) \right) + C_1 \\
&\le C_2 \lim_{r\to 0+} \Big((\mathrm{diam}(\Omega) - r) \ln|\mathrm{diam}(\Omega)| + C_2 r \ln|r| \Big) + C_1 \\
&= C_2 \mathrm{diam}(\Omega) \ln|\mathrm{diam}(\Omega)| + C_1 < +\infty, \qquad (8)
\end{aligned}$$

where $\mathrm{diam}(\Omega)$ denotes the diameter of Ω.

For $\mathcal{I}_1$, we begin with the following approximation

$$\frac{\partial\Phi(y,x)}{\partial\nu(x)} \approx j\omega\Phi(y,x).$$

Then applying integration by parts yields

$$\begin{aligned}
\mathcal{I}_1 &= \int_{\partial\Omega} \Phi(y,x)\Phi(z,x) dS(x) = \frac{1}{j\omega} \int_{\partial\Omega} \frac{\partial\Phi(y,x)}{\partial\nu(x)} \Phi(z,x) dS(x) \\
&= \frac{1}{j\omega} \int_\Omega \left(\triangle + \omega^2\right) \Phi(y,x)\Phi(z,x) dx + \frac{1}{j\omega} \int_{\partial\Omega} \Phi(y,x) \frac{\partial\Phi(z,x)}{\partial\nu(x)} dS(x).
\end{aligned}$$

Then by the definition of $\Phi(y, x)$ and similar argument of (8), $\mathcal{I}_1$ can be estimated as follows

$$\mathcal{I}_1 = \frac{j}{\omega}\Phi(y,z) + C_3 = \frac{1}{4\omega} H_0^1(\omega|y-z|) + C_3.$$

Therefore, by combining the results of $\mathcal{I}_l$, $l = 1, 2, 3, 4$,

$$\int_{\partial\Omega} \mathcal{N}(y,x)\mathcal{N}(z,x) dS(x) \approx \frac{j}{\omega}\Phi(y,z) + \hat{C}.$$

Now, let us consider the case of plane-wave illumination, i.e., we set the boundary condition $g^{(m)}(x)$, $m = 1, 2, \ldots, M$ as

$$g^{(m)}(x) = \frac{\partial \exp(j\omega\theta_m \cdot x)}{\partial \nu(x)} = \Big(j\omega\theta_m \cdot \nu(x)\Big) \exp(j\omega\theta_m \cdot x).$$

Then since $U^{(m)}(y) = \exp(j\omega\theta_m \cdot y)$, (7) becomes

$$d_T\mathbb{J}(z) \approx -\mathfrak{Re}\left\{\frac{j}{\omega}\sum_{m=1}^{M} \exp\Big(j\omega\theta_m \cdot (y-z)\Big)\Phi(y,z)\right\}. \tag{9}$$

Notice that if the value of M is large enough, following approximation holds

$$\frac{1}{M}\sum_{m=1}^{M} \exp\big(j\omega\theta_m \cdot (y-z)\big) \approx J_0(\omega|y-z|), \tag{10}$$

where J_0 is the Bessel function of order zero and of the first kind. Therefore, $d_T\mathbb{J}(z)$ becomes

$$d_T\mathbb{J}(z) \simeq -J_0(\omega|y-z|)^2, \tag{11}$$

where $A \simeq B$ means that there exist a constant C satisfying $A = BC$. With this, we end up this section with the following remark.

Remark 3.1 *From the structure (9), we can observe following:*

- $J_0(x)$ *has its maximum value at* $x = 0$ *so that* $d_T\mathbb{J}(z)$ *reaches its minimum value at* $z = y \in \Gamma$ *due to the minus sign in (11).*
- *Based on (10), when the number* M *is getting larger, we can find more exact location and shape of cracks by looking at the points of minimal values in the map of* $d_T\mathbb{J}(z)$.
- *Due to the assumption of* $\mathrm{dist}(\Gamma, \partial\Omega) \geq s$, *map of* $d_T\mathbb{J}(z)$ *plots the crack far away from boundary* $\partial\Omega$, *i.e., when the location of crack is close to the boundary it cannot be imaged in theory.*

4. NUMERICAL SIMULATIONS

Some numerical examples are performed for showing the effectiveness of imaging algorithm. Throughout this section, the domain Ω is chosen as the two-dimensional unit disk centered at the origin. We adopt the applied frequency as $\omega = 2\pi/\lambda$ at wavelength λ and choose M equi-distributed incident directions

$$\theta_m := \left(\cos\frac{2m\pi}{M}, \sin\frac{2m\pi}{M}\right) \quad \text{for} \quad m = 1, 2, \ldots, M.$$

Let us emphasize that every simulations are performed by the measurements using the Finite Element Method (FEM) in order to

solve the problems (2) and (6). Then, a white Gaussian noise with 20 dB signal-to-noise ratio (SNR) is added to the unperturbed data.

Now, we consider the imaging of two small cracks are completely embedded in Ω. Their locations are selected as $z_1 = (-0.5, -0.2)$ and $z_2 = (0.5, 0.2)$ and lengths are set to 0.02. Figure 2 shows the map of $d_T\mathbb{J}(z)$ when $\lambda = 0.5$. Although, $d_T\mathbb{J}(z)$ plots its minimum at z_1 and z_2, a number of weak replicas are also plotted when $M = 4$ (see Figure 2(a)). In order to eliminate them, based on second part of Remark 3.1, one must apply a large number of M. In this case, $M = 8$ is a good choice, refer to Figure 2(b). Figure 2(c) shows the imaging result when the length of cracks are extremely small (such as point-like scatterers) $h = 10^{-9}$. Although, this algorithm works for point-like scatterers in theory, it is hard to recognize the location of them due to the points of small magnitudes.

Based on the recent research [3], considering the Rayleigh resolution limit, proposed algorithm can be applied to the imaging of arbitrary shaped, curve-like perfectly conducting cracks. In order to perform numerical simulation, four curves are chosen for illustration of crack:

$$\begin{aligned}
\Gamma_1 &= \left\{\left(s - 0.2, -0.5s^2 + 0.6\right) : s \in [-0.5, 0.5]\right\} \\
\Gamma_2 &= \left\{\left(s + 0.2, s^3 + s^2 - 0.6\right) : s \in [-0.5, 0.5]\right\} \\
\Gamma_3 &= \left\{\left(0.6s, 0.5\cos\frac{s\pi}{2} + 0.5\sin\frac{\pi s}{2} - 0.1\cos\frac{3\pi s}{2}\right) : s \in [-1, 1]\right\}. \\
\Gamma_4 &= \left\{\left(1.5\sin\frac{(3s+4)\pi}{9} - 1,\ 0.8\sin\frac{(3s+4)\pi}{4}\right) : s \in [-1, 1]\right\}.
\end{aligned}$$

Let us consider the imaging result of Γ_1 with operating wavelength $\lambda = 0.5$. Corresponding result is exhibited in Figure 3. Similar to the small cracks case, we can easily notice that when the value of M is small, it is hard to recognize the true shape of Γ_1, refer to Figure 3(a). However, if we adopt a large number of $M = 16$, 24 or 32, $d_T\mathbb{J}(z)$

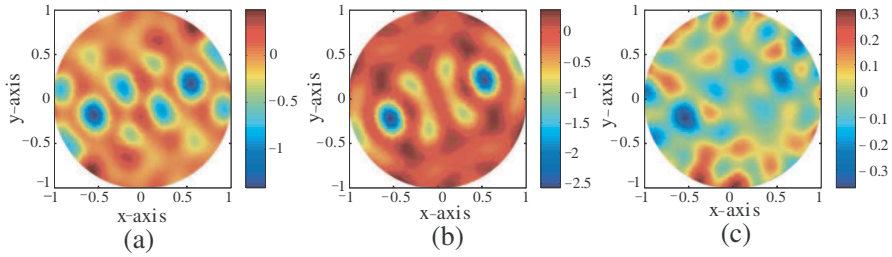

Figure 2. Map of $d_T\mathbb{J}(z)$ for two small cracks when $\lambda = 0.5$. (a) For $M = 4$. (b) For $M = 8$. (c) For $M = 8$ and $h = 10^{-9}$.

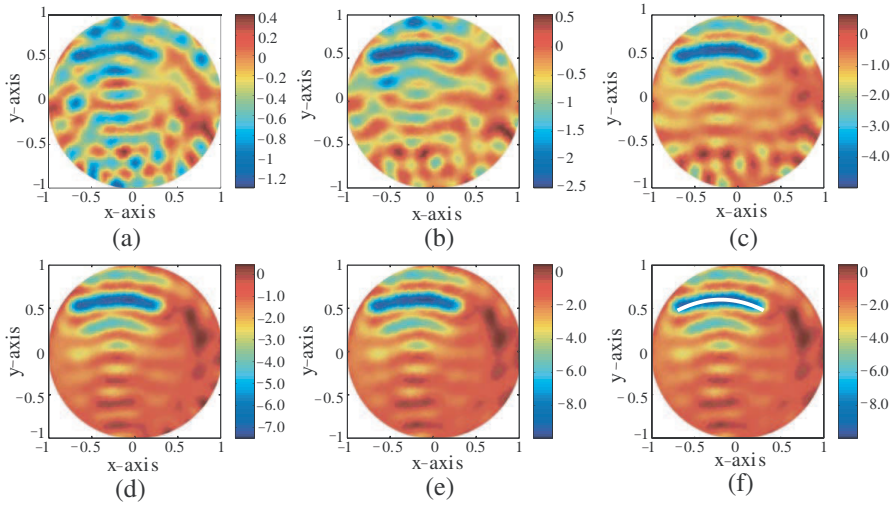

Figure 3. Map of $d_T\mathbb{J}(z)$ for Γ_1 when $\lambda = 0.5$. (a) For $M = 4$. (b) For $M = 8$. (c) For $M = 16$. (d) For $M = 24$. (e) For $M = 32$. (f) True shape

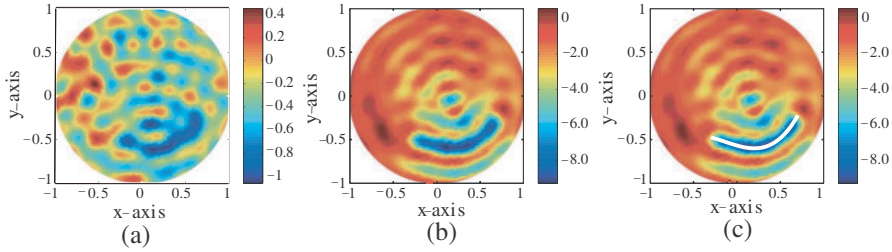

Figure 4. Map of $d_T\mathbb{J}(z)$ for Γ_2 when $\lambda = 0.5$. (a) For $M = 4$. (b) For $M = 32$. (c) True shape.

reaches its minimum values in the neighborhood of Γ_1. Similarly, an image with good resolution has appeared when the crack is Γ_2 by regarding Figure 4.

At this stage, let us compare the imaging performance. Figures 5(b) and (c) show the imaging results of proposed algorithm and MUSIC-type one (see [5, 24]), respectively. Notice that in Figure 5(b), some parts of Γ_3 cannot be imaged, i.e., proposed algorithm offers better result than MUSIC-type one in this experiment.

Let us apply proposed algorithm for imaging of multiple, non-overlapping extended cracks $\Gamma_1 \cup \Gamma_2$. Similar to the imaging of single

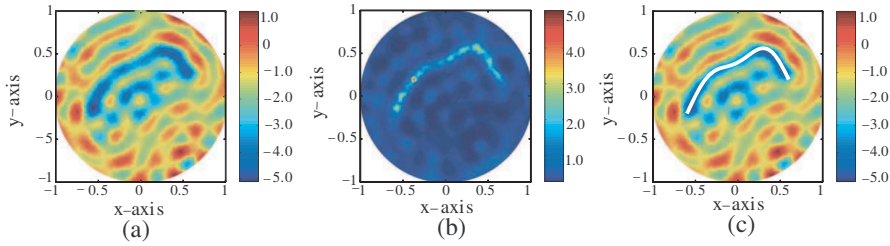

Figure 5. Imaging result of Γ_3 when $\lambda = 0.5$ and $M = 16$. (a) Via proposed algorithm. (b) Via MUSIC. (c) True shape.

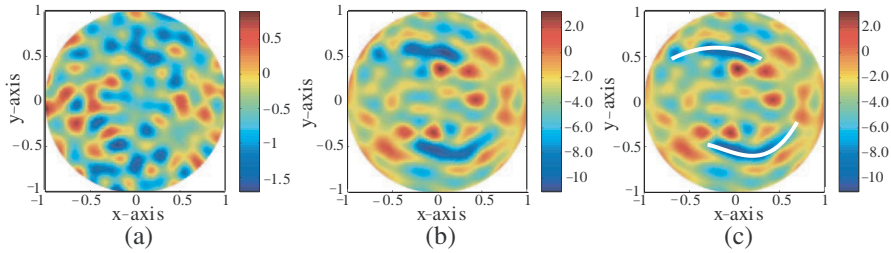

Figure 6. Map of $d_T\mathbb{J}(z)$ for $\Gamma_1 \cup \Gamma_2$ when $\lambda = 0.5$. (a) For $M = 4$. (b) For $M = 32$. (c) True shape.

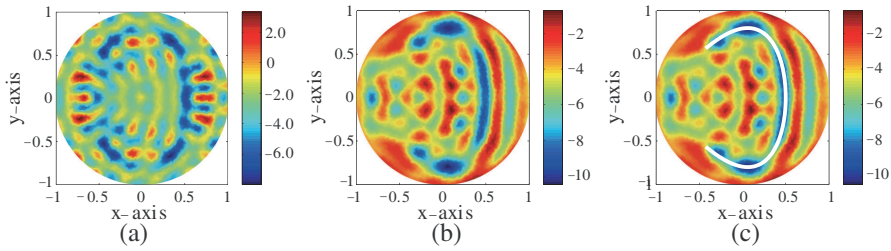

Figure 7. Map of $d_T\mathbb{J}(z)$ for Γ_4 when $\lambda = 0.5$. (a) For $M = 16$. (b) For $M = 32$. (c) True shape.

crack, one cannot recognize the shape of cracks for small number of M. In order to obtain a good result, we must apply $M = 32$ (or more) number of different incident directions, refer to Figure 6.

Now, let us consider the imaging of crack which has a lower radius of curvature. Figure 7 shows the imaging result of Γ_4. Note that the location of Γ_4 is more closer than Γ_k, $k = 1, 2, 3$. Although, we applied $M = 32$ different directions, an image with poor resolution is appeared. This experiment shows the limitation of proposed algorithm.

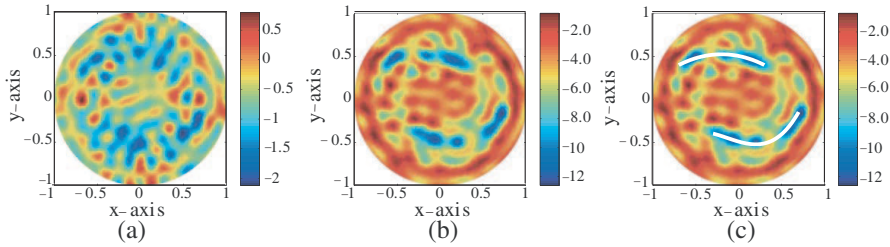

Figure 8. Map of $d_T\mathbb{J}(z)$ for $\Gamma_1 \cup \Gamma_2$ when $\lambda = 0.4$. (a) For $M = 4$. (b) For $M = 32$. (c) True shape.

At the final stage, let us consider when the measured boundary data is significantly affected by the random noise. The imaged cracks are selected by the moved one of Γ_1 and Γ_2, as previously introduced. Figure 8 shows the map of $d_T\mathbb{J}(z)$ with operating wavelength $\lambda = 0.4$ when a white Gaussian noise with 10 dB signal-to-noise ratio (SNR) is added to the unperturbed boundary data. In this case, although M is large enough, it is very hard to obtain a good result. This result shows the limitation of proposed algorithm.

5. CONCLUSION

In this paper, a topological derivative based non-iterative algorithm has been considered for imaging small and extended perfectly conducting cracks completely hidden in the two-dimensional homogeneous domain Ω. Based on the asymptotic expansion formula, the structure of such derivative has been analyzed and tells us the number of different incident direction must be large enough for obtaining a reliable image of crack(s). Various numerical examples show that proposed algorithm is fast and stable for imaging of cracks so that obtained results could provide good initial guesses for the traditional Newton-type iterative algorithms or a level-set methods [1, 17, 19, 25].

We have considered in the case of perfectly conducting crack with Dirichlet boundary condition, extension to the crack with Neumann boundary condition case is also an interesting subject. In practice, it is very hard to increase the number of incident direction M so that development of an improved imaging algorithm with a small number of M will be a forthcoming work. Finally, we believe that proposed algorithm can be applied in the practical applications for example, semiconductor industry to detect the cracks in silicon wafer. We will try to apply it to the real world applications.

ACKNOWLEDGMENT

W.-K. Park would like to thank Habib Ammari for many valuable advices. The authors gratefully acknowledge to the anonymous reviewers for their valuable comments. Y.-K. Ma was supported by the National Research Foundation of Korea (NRF) grant funded by the Korea government (MEST) (No. 2011-0030810). P.-S. Kim was supported by the research program 2012 of Kookmin University in Korea. W.-K. Park was supported by the research program 2012 of Kookmin University in Korea and the WCU (World Class University) program through the National Research Foundation of Korea (NRF) funded by the Ministry of Education, Science and Technology R31-10049.

APPENDIX A. APPENDIX: PROOF OF THEOREM 2.1

Let Σ be a small crack of length $2h$ and $W^{(m)}(x)$ satisfies the following boundary value problem:

$$\begin{cases} \triangle W^{(m)}(x) + \omega^2 W^{(m)}(x) = 0 & \text{in} \quad \Omega \backslash \overline{\Sigma} \\ W^{(m)}(x) = 0 & \text{on} \quad \Sigma \\ \dfrac{\partial W^{(m)}}{\partial \nu}(x) = g^{(m)}(x) & \text{on} \quad \partial\Omega. \end{cases} \tag{A1}$$

Then, by virtue of [5], $W^{(m)}(x)$ can be written as follows: for $x \in \partial\Omega$,

$$W^{(m)}(x) - U^{(m)}(x) = \frac{2\pi}{\ln(h/2)} U^{(m)}(z)\mathcal{N}(x,z) + O\left(\frac{1}{|\ln h|^2}\right). \tag{A2}$$

Let us examine the relationship between $\mathbb{J}(\Omega|\Sigma)$ and $\mathbb{J}(\Omega)$ as follows:

$$\begin{aligned} \mathbb{J}(\Omega|\Sigma) &= \frac{1}{2}\sum_{m=1}^{M}\int_{\partial\Omega}\left|W^{(m)}(x) - u^{(m)}(x)\right|^2 dS(x) \\ &= \frac{1}{2}\sum_{m=1}^{M}\int_{\partial\Omega}\left|W^{(m)}(x) - U^{(m)}(x) + U^{(m)}(x) - u^{(m)}(x)\right|^2 dS(x) \\ &= \frac{1}{2}\sum_{m=1}^{M}\int_{\partial\Omega}\left(\left|U^{(m)}(x) - u^{(m)}(x)\right|^2 + \left|W^{(m)}(x) - U^{(m)}(x)\right|^2\right) dS(x) \\ &\quad + \sum_{m=1}^{M}\int_{\partial\Omega}\left(U^{(m)}(x) - u^{(m)}(x)\right)\left(\overline{W^{(m)}(x) - U^{(m)}(x)}\right) dS(x) \\ &= \mathbb{J}(\Omega) + \sum_{m=1}^{M}\mathbb{F}(z) + O\left(\frac{1}{|\ln h|^2}\right), \end{aligned}$$

where

$$\mathbb{F}(z) = \int_{\partial\Omega} \left(U^{(m)}(x) - u^{(m)}(x) \right) \left(\overline{W^{(m)}(x) - U^{(m)}(x)} \right) dS(x).$$

Applying asymptotic formula (13) and boundary condition in (6), $\mathbb{F}(z)$ can be written

$$\mathbb{F}(z) = \int_{\partial\Omega} \frac{\partial V^{(m)}}{\partial \nu}(x) \left(\overline{\frac{2\pi}{\ln(h/2)} U^{(m)}(z)\mathcal{N}(x,z)} \right) dS(x).$$

Through the integration by parts process, we can calculate following equalities

$$\begin{aligned}
&\int_{\partial\Omega} \frac{\partial V^{(m)}}{\partial \nu}(x) \left(\overline{U^{(m)}(z)\mathcal{N}(x,z)} \right) dS(x) \\
&= \int_{\Omega} \left(\triangle V^{(m)}(x) \overline{U^{(m)}(z)\mathcal{N}(x,z)} + \nabla V^{(m)}(x) \cdot \overline{U^{(m)}(z) \nabla \mathcal{N}(x,z)} \right) dx \\
&= \int_{\Omega} \left(\triangle V^{(m)}(x) \overline{U^{(m)}(z)\mathcal{N}(x,z)} + \omega^2 V^{(m)}(x) \overline{U^{(m)}(z)\mathcal{N}(x,z)} \right) dx \\
&\quad - \int_{\Omega} \left(V^{(m)}(x) \overline{U^{(m)}(z) \triangle \mathcal{N}(x,z)} + \omega^2 V^{(m)}(x) \overline{U^{(m)}(z)\mathcal{N}(x,z)} \right) dx \\
&= \int_{\Omega} \left((\triangle + \omega^2) V^{(m)}(x) \right) \overline{U^{(m)}(z)\mathcal{N}(x,z)} dx \\
&\quad - \int_{\Omega} V^{(m)}(x) \overline{U^{(m)}(z) \left((\triangle + \omega^2)\mathcal{N}(x,z) \right)} dx = V^{(m)}(z) \overline{U^{(m)}(z)}.
\end{aligned}$$

Therefore,

$$\mathbb{J}(\Omega|\Sigma) = \mathbb{J}(\Omega) + \frac{2\pi}{\ln(h/2)} \sum_{m=1}^{M} V^{(m)}(z) \overline{U^{(m)}(z)} + O\left(\frac{1}{|\ln h|^2} \right).$$

By taking real part of above identity, theorem 2.1 can be derived. This ends the proof.

REFERENCES

1. Álvarez, D., O. Dorn, N. Irishina, and M. Moscoso, "Crack reconstruction using a level-set strategy," *J. Comput. Phys.*, Vol. 228, 5710–5721, 2009.
2. Ammari, H., *An Introduction to Mathematics of Emerging Biomedical Imaging*, Mathematics and Applications Series, Vol. 62, Springer-Verlag, Berlin, 2008.

3. Ammari, H., E. Bonnetier, and Y. Capdeboscq, "Enhanced resolution in structured media," *SIAM J. Appl. Math.*, Vol. 70, 1428–1452, 2009.
4. Ammari, H. and H. Kang, *Reconstruction of Small Inhomogeneities from Boundary Measurements*, Lecture Notes in Mathematics, Vol. 1846, Springer-Verlag, Berlin, 2004.
5. Ammari, H., H. Kang, H. Lee, and W.-K. Park, "Asymptotic imaging of perfectly conducting cracks," *SIAM J. Sci. Comput.*, Vol. 32, 894–922, 2010.
6. Amstutz, S., I. Horchani, and M. Masmoudi, "Crack detection by the topological gradient method," *Control and Cybernetics*, Vol. 34, 81–101, 2005.
7. Auroux, D. and M. Masmoudi, "Image processing by topological asymptotic analysis," *ESAIM: Proc.*, Vol. 26, 24–44, 2009.
8. Bonnet, M., "Fast identification of cracks using higher-order topological sensitivity for 2-D potential problems," *Eng. Anal. Bound. Elem.*, Vol. 35, 223–235, 2011.
9. Byrne, D., M. O'Halloran, M. Glavin, and E. Jones, "Data independent radar beamforming algorithms for breast cancer detection," *Progress In Electromagnetic Research*, Vol. 107, 331–348, 2010.
10. Carpio, A. and M.-L. Rapun, "Solving inhomogeneous inverse problems by topological derivative methods," *Inverse Problems*, Vol. 24, 045014, 2008.
11. Chen, G. P. and Z. Q. Zhao, "Ultrasound tomograohy-guide TRM technique for breast tumor detecting in MITAT system," *Journal of Electromagnetic Waves and Applications*, Vol. 24, Nos. 11–12, 1459–1471, 2010.
12. Chen, X., "Subspace-based optimization method in electric impedance tomography," *Journal of Electromagnetic Waves and Applications*, Vol. 23, Nos. 11–12, 1397–1406, 2009.
13. Colton, K. and R. Kress, *Inverse Acoustic and Electromagnetic Scattering Theory*, Applied Mathematical Sciences, Vol. 93, Springer, Berlin, 1998.
14. Conceição, R. C., M. O'Halloran, M. Glavin, and E. Jones, "Numerical modelling for ultra wideband radar breast cancer detection and classification," *Progress In Electromagnetic Research B*, Vol. 34, 145–171, 2011.
15. Donelli, M., "A rescue radar system for the detection of victims trapped under rubble based on the independent component analysis algorithm," *Progress In Electromagnetic Research M*, Vol. 19, 173–181, 2011.

16. Donelli, M., I. J. Craddock, D. Gibbins, and M. Sarafianou, "A three-dimensional time domain microwave imaging method for breast cancer detection based on an evolutionary algorithm," *Progress In Electromagnetic Research M*, Vol. 18, 179–195, 2011.
17. Dorn, O. and D. Lesselier, "Level set methods for inverse scattering," *Inverse Problems*, Vol. 22, R67–R131, 2006.
18. Eschenauer, H. A., V. V. Kobelev, and A. Schumacher, "Bubble method for topology and shape optimization of structures," *Struct. Optim.*, Vol. 8, 42–51, 1994.
19. Kress, R., "Inverse scattering from an open arc," *Math. Methods Appl. Sci.*, Vol. 18, 267–293, 1995.
20. Kuo, W.-C., C.-Y. Chuang, M.-Y. Chou, W.-H. Huang, and S.-T. Cheng, "Phase detection with sub-nanometer sensitivity using polarization quadrature encoding method in optical coherence tomography," *Progress In Electromagnetic Research*, Vol. 104, 297–311, 2010.
21. Lesselier, D. and B. Duchene, "Buried, 2-D penetrable objects illuminated by line sources: FFT-based iterative computations of the anomalous field," *Progress In Electromagnetic Research*, Vol. 5, 351–389, 1991.
22. O'Halloran, M., M. Glavin, and E. Jones, "Rotating antenna microwave imaging system for breast cancer detection," *Progress In Electromagnetic Research*, Vol. 107, 203–217, 2010.
23. Park, W.-K., "On the imaging of thin dielectric inclusions via topological derivative concept," *Progress In Electromagnetic Research*, Vol. 110, 237–252, 2010.
24. Park, W.-K. and D. Lesselier, "Electromagnetic MUSIC-type imaging of perfectly conducting, arc-like cracks at single frequency," *J. Comput. Phys.*, Vol. 228, 8093–8111, 2009.
25. Park, W.-K. and D. Lesselier, "Reconstruction of thin electromagnetic inclusions by a level set method," *Inverse Problems*, Vol. 25, 085010, 2009.
26. Sokołowski, J. and A. Zochowski, "On the topological derivative in shape optimization," *SIAM J. Control Optim.*, Vol. 37, No. 4, 1251–1272, 1999.
27. Zhou, Y., "Microwave imaging based on wideband range profiles," *Progress In Electromagnetics Research Letters*, Vol. 19, 57–65, 2010.
28. Zhu, G. K. and M. Popovic, "Comparison of radar and thermoacoustic technique in microwave breast imaging," *Progress In Electromagnetics Research B*, Vol. 35, 1–14, 2011.